Supporting Information for

Upgraded Decatungstate: The Visible-Light-Responsive, Recyclable, and Efficient Photocatalyst Achieved via Self-Assembly

Yanan Liu†[a,b], Luoning Li†[a], Minzhen Cai[a], Jing Wang[a], Pengtao Ma[a], Jingping Wang[a,*], and Jingyang Niu[a,*]

[a] Henan Key Laboratory of Polyoxometalate Chemistry, College of Chemistry and Molecular Sciences, Henan University, Kaifeng, Henan, 475004 (P. R. China).

[b] Puyang Institute of Technology, Henan University, Puyang, Henan, 457000 (P. R. China).

Corresponding Authors: jpwang@henu.edu.cn (J.P. Wang); jyniu@henu.edu.cn (J.Y. Niu).

Table of Contents

Section S1 Experimental Section **Pages S2**

Section S2 Supplementary Tables Section **Pages S6**

Section S3 Supplementary Figures Section **Pages S9**

Section S4 References **Pages S20**

Section S1 Experimental Section

1. Materials and characterizations.

All chemicals were reagent grade quality obtained from commercial sources and used without any further purification. The precursor decatungstate ($TBA_4[W_{10}O_{32}]$, TBADT) were synthesized according to the literature[1,2] and further confirmed by Fourier transform infrared spectroscopy (FTIR). FTIR spectra were conducted on a Bruker VERTEX 70 IR spectrometer (KBr pellets) recording in the range of 4000−450 cm^{-1}. Powder X-ray diffraction (PXRD) patterns were obtained by employing a Bruker D8 ADVANCE diffractometer with Cu Kα radiation (the value of λ is 1.54056 Å). Thermogravimetric Analysis (TGA) were measured by a Perkin-Elmer TGA7 instrument under flowing N_2 (heating rate, 10 °C·min^{-1}). Elemental analyses (C, H, N, O) were conducted on an Elementar Vario MICRO analyzer. The quantitative analyses of Cd, Ru and W elements were achieved by Agilent 5110 inductively coupled plasma optical emission spectrometer (ICP-OES). Transmission electron microscopy (TEM) images and elemental mapping were obtained by the JEM-F200. X-ray photoelectron spectroscopy (XPS) was performed with an Axis Ultra X-ray photoelectron spectroscope equipped with monochromatic Al Kα (1486.7 eV) radiation. The UV-vis diffuse reflectance spectroscopy (UV-vis-DRS) analysis was conducted with a Cary 5000 UV-Vis-NIR spectrophotometer using $BaSO_4$ powder as the reference. The steady-state photoluminescence (PL) spectra and the time-resolved PL decay spectra were recorded on a photoluminescence spectrometer (Edinburgh FLS1000) using picosecond pulsed diode lasers (375 nm) as the excitation sources. The ^1H NMR spectra of $[Ru(bpy)_2(H_2dcbpy)]Cl_2$ are relative to DMSO (d = 2.5 ppm), and the ^1H and ^{13}C NMR spectra of typical catalytic products are chemical shifts relative to $CDCl_3$ (d = 7.26 ppm and 77.2 ppm). The photocatalytic reactions were performed on WATTCAS Parallel Light Reactor (WP-TEC-1020HSL) with a 10 W COB LED. The products were confirmed by GC−MS (Agilent 7890B GC/5977B MS, SE-54 capillary column) and the yield was calculated by GC on Agilent 8890.

2. X-ray crystallography.

The single crystals **CR-DT** were directly fixed on a loop and kept at 150 K during data collection on a Bruker D8 VENTURE PHOTON II CCD diffractometer with Mo Kα radiation (the value of λ is 0.71073 Å). The structure was solved with the ShelXT structure solution program using Intrinsic Phasing and further refined by the full-matrix least-squares method on F^2 using the ShelXL refinement package within Olex2.[3] All the atoms were refined anisotropically in the final refinement cycle, only a few harsh constraints have been used to eliminate the ADP alert of a few atoms. And some disorders DMF were determined by the TGA results and element analyses. Crystallographic data of **CR-DT** have been deposited in the Cambridge Crystallographic Data Center with CCDC number of 2374016. The crystallographic data and structure refinement parameters of **CR-DT** are shown in Table S1−3.

3. Electrochemical measurements.

Every electrochemical study was carried out using a standard three-electrode setup at ambient temperatures on an electrochemical workstation (CHI-760E, Shanghai, China). The 0.2 M Na_2SO_4 aqueous solution served as the electrolyte solution, the Pt wire served as the counter electrode, and the Ag/AgCl electrode served as the reference electrode. To create a working electrode, 470 μL of ethanol and 30 μL of Nafion were added to the 5 mg ground sample. After 1 h of ultrasound treatment, 30 μL of the evenly mixed suspension was extracted using a micro-sampler and evenly coated on a 2 cm × 1 cm FTO conductive glass surface. After drying naturally at room temperature, the FTO is fixed on the glass carbon electrode clamp to make the working electrode. Before the test, the solution was injected with high-purity nitrogen for over 30 min. After this, the Mott−Schottky diagram, photocurrent time (I-t) curve, and electrochemical impedance (EIS) were measured under a nitrogen atmosphere. It should be pointed out

that the I-t curve was measured with a 300 W xenon lamp (Beijing China Education Au-Light Technolgy Co. Ltd., CEL-PF300-T10) source intermittently irradiating the sample.

4. Synthesis of $[Ru(bpy)_2(H_2dcbpy)]Cl_2$

$[Ru(bpy)_2(H_2dcbpy)]Cl_2$ was synthesized according to the published synthesis procedure with some modifications.[4,5] $[Ru(bpy)_2Cl_2]$ (800 mg,1.65 mmol) and (2,2'-bipyridine)-5,5'-dicarboxylic acid (505 mg, 2.1 mmol) were mixed in 100 mL of EtOH/H_2O (1:1, v/v), and refluxed for 24 hours under Ar atmosphere. After cooling to room temperature the solvents were removed, and the solid was recrystallized from 100 mL of MeOH/diethyl ether (1:1, v/v) mixture. ^{1}H NMR (500 MHz, DMSO-d_6, ppm): δ 9.07 (d, J = 8.4 Hz, 2H), 8.97 (d, J = 8.1 Hz, 2H), 8.93 (d, J = 8.2 Hz, 2H), 8.62 – 8.57 (m, 2H), 8.31 (t, J = 7.9 Hz, 2H), 8.25 (t, J = 7.9 Hz, 2H), 8.10 – 8.06 (m, 2H), 7.93 (d, J = 5.8 Hz, 2H), 7.86 (d, J = 5.4 Hz, 2H), 7.80 (d, J = 5.4 Hz, 1H), 7.70 – 7.66 (m, 2H), 7.61 – 7.56 (m, 2H).

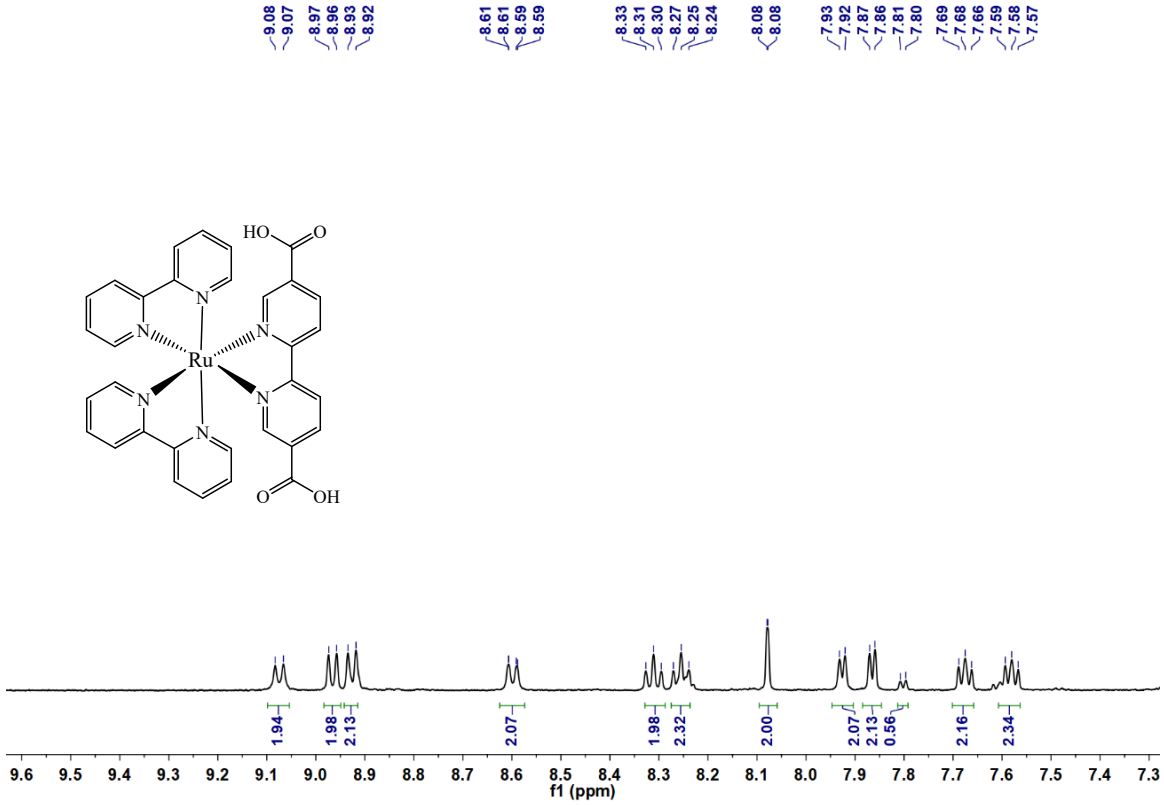

Fig. S1. ^{1}H NMR spectrum of $[Ru(bpy)_2(H_2dcbpy)]Cl_2$ in DMSO-d_6.

5. The calculation of parameters for the assessment of catalyst performance.

5.1 The calculation of Turnover number (TON) and Turnover frequency (TOF).

$$TON = \frac{n_p}{n_c} \qquad TOF = \frac{n_p}{n_c \cdot t}$$

where n_p is the molar amounts of the product (mol); n_c is the molar amounts of the catalyst (mol); t is reaction time (h). Test conditions for TOF: **CR-DT** (1 μmol), cyclohexanone (1 mmol), benzaldehyde (2 mmol), 1,2-dichloroethane (1 mL), O_2 (1 atm), and 10 W white LED lamp. And the yield of ε-caprolactone was 11.3% after 10 min.

5.2 The calculation of apparent quantum yield (AQY).

The AQY is determined using a similar method to that for the photocatalytic performance test. **CR-DT** (1 μmol), cyclohexanone (1 mmol), benzaldehyde (2 mmol), 1,2-dichloroethane (2 mL), O_2 (1 atm), and 10 W 465 nm LED lamp. The intensity of the incident light was 47.9 mW·cm^{-2}, which was tested by a photometer (CEL-NP2000-2A, Beijing CEAulight Co., Ltd., China), the irradiated area is 2 cm^2. The yield of ε-caprolactone was 18.87% after 28 min.

$$AQY\% = \frac{amounts\ of\ products\ formed}{amounts\ of\ photons\ irradiated} \times 100\%$$

$$= \frac{N_e}{N_p} = \frac{nN_A/t}{IS/hv} = \frac{nN_A hc}{IS\lambda t} \times 100\%$$

N_e represents the amounts of products formed;

N_p represents the amounts of photons irradiated;

n is the molar amounts of product formed (mol);

t is the reaction time (s);

N_A is Avogadro constant (6.022×10^{23} mol^{-1});

I is the incident light intensity at certain wavelength (W·m^{-2});

S is the irradiated area (m^2);

h is Planck constant (6.626×10^{-34} J·s);

c is the speed of light (2.998×10^{8} m·s^{-1});

λ is the wavelength of incident light (m).

6. Mechanistic study of photocatalytic Baeyer–Villiger oxidation of cyclohexanone.

6.1 Stern–Volmer quenching experiments.

In a typical experiment, 1 mg of ground **CR-DT** was weighed and added to 2 mL of Dimethyl sulfoxide (DMSO) solution, and the suspension was sonicated for 20 min. Different concentrations of benzaldehyde were added to the suspension and mixed well before the test. The solution to be measured was added to a 3 mL cuvette and placed in a fluorescence spectrophotometer (Edinburg, FLS-1000), and its emission spectrum (excitation at 223 nm, recording at 430 nm) was measured at room temperature.

6.2 Electron paramagnetic resonance (EPR) measurement of the radicals.

General procedure of the EPR measurement: **CR-DT** (1 μmol), benzaldehyde (2 mmol), 1,2-dichloroethane (2 mL) and N-tert-butyl-α-phenylnitrone (PBN, 0.2 mmol) were added to the glass vial and mixed with stirring. Then, the solutions under dark and after light exposure for 10 min were aspirated into glass capillaries, respectively, and the capillaries were placed in the hole of acceptor. Then, the EPR spectra were monitored using a Bruker EMXPLUS. Measurement settings were as follows: modulation frequency, 100 kHz; sweep time, 30 s; microwave power, 6.325 mW; microwave frequency, 9.85 GHz.

Section S2 Supplementary Tables Section

Table S1. Crystallographic data structure refinement for **CR-DT**.

Crystal Data	CR-DT
Empirical formula	$C_{64}H_{44}Cd_2N_{12}O_{44}Ru_2W_{10}$
Formula weight	3950.55
Temperature/K	150.0
Crystal system	orthorhombic
Space group	*Cmce*
a/Å	28.625(19)
b/Å	20.427(11)
c/Å	24.967(19)
α/°	90
β/°	90
γ/°	90
Volume/Å^3	14600(16)
Z	4
ρ_{calc}g/cm^3	1.797
μ/mm^{-1}	8.386
F(000)	7152.0
Crystal size/mm^3	0.27 × 0.19 × 0.07
Radiation	MoKα (λ = 0.71073)
2θ range for data collection/°	4.9 to 50.2
Index ranges	$-32 \le h \le 34$, $-24 \le k \le 24$, $-29 \le l \le 29$
Reflections collected	62824
Independent reflections	6629 [R_{int} = 0.0650, R_{sigma} = 0.0314]
Data/restraints/parameters	6629/84/275
Goodness-of-fit on F^2	1.044
Final R indexes [I>=2σ (I)]	R_1 = 0.0392, wR_2 = 0.0939
Final R indexes [all data]	R_1 = 0.0533, wR_2 = 0.1017
Largest diff. peak/hole / e Å^{-3}	1.53/-1.19

$R_1 = \sum||Fo| - |Fc||/\sum|Fo|$, $wR_2 = [\sum w(Fo^2 - Fc^2)^2/\sum w(Fo^2)^2]^{1/2}$

Table S2. The hydrogen bonds of **CR-DT**.

D−H…A	d(H…A)	d(D…A)	<(DHA)
C3−H3…O6	2.430	3.299	151.90
C4−H4…O4	2.500	3.406	159.29
C7−H7…O2	2.420	3.171	135.83

Table S3. The selected bond lengths of **CR-DT**.

Bond	Length (Å)	Bond	Length (Å)
W1−O5	2.308(4)	W3−O4[3]	1.890(6)
W1−O1	1.928(4)	W3−O4	1.890(6)
W1−O7	1.926(5)	W3−O6	1.726(8)
W1−O3	1.869(5)	N1−C5	1.3900
W1−O4	1.991(6)	N1−C1	1.3900
W1−O2	1.697(5)	N1−Ru1	2.057(5)
N3−C15	1.3900	C5−C4	1.3900
N3−C11	1.3900	C5−C6	1.406(9)
N3−Ru1	2.058(5)	C4−C3	1.3900
C15−C14	1.3900	C3−C2	1.3900
C14−C13	1.3900	C2−C1	1.3900
C14−C16	1.518(16)	Ru1−N2[1]	2.042(5)
C13−C12	1.3900	Ru1−N2	2.042(5)
C12−C11	1.3900	C7−C6	1.3900
C11−C11[1]	1.429(12)	C7−C8	1.3900
W2−O5	2.324(4)	C6−N2	1.3900
W2−O7	1.916(5)	N2−C10	1.3900
W2−O9	1.928(4)	C10−C9	1.3900
W2−O3[2]	1.927(5)	C9−C8	1.3900
W2−O8	1.922(5)	O11−C16	1.214(14)
W2−O10	1.694(6)	O11−Cd1	2.337(10)
W3−O5	2.288(6)	O12−C16	1.222(14)
W3−O8[3]	1.942(6)	O12−Cd1	2.379(9)
W3−O8	1.942(6)		

[1]+X,1-Y,1-Z; [2]+X,-Y,1-Z; [3]1-X,+Y,+Z

Table S4. The parameters from fitting the TRPL decay profiles of **CR-DT**, H_2L and DT.

Samples	τ_1 (ns)	A_1	τ_2 (ns)	A_2	τ_{avg} (ns)	R^2
CR-DT	1.09065	1040.76045	6.95876	92.1505	3.21	0.99136
H_2L	0.91628	1013.60404	5.98785	97.56804	2.87	0.99338
DT	0.66103	927.23471	4.48411	118.20088	2.43	0.99679

Table S5. Comparison of the activity with previously reported photocatalysts.

Entry	Catalyst	Oxidant	Light source	t (h)	Yield (%)	TON/TOF (h^{-1})	AQY (%)	Ref
1	**CR-DT**	O_2/aldehyde	10W white LED lamp (>400 nm)	4	99.5	995/678	4.69	This work
2	CR-SiW_{12}	O_2/aldehyde	10W white LED lamp (>400 nm)	3	94.1	941/274.5	8.4	6
3	Ru-NiMo	O_2/aldehyde	10W white LED lamp (>400 nm)	3	95.5	955/440	4.4	7
4	Ru-Mo_8	O_2/aldehyde	10W white LED lamp (>400 nm)	3	96.7	967/548	6.84	8
5	1	O_2/aldehyde	10W white LED lamp (>400 nm)	3	95.1	951/510	2.7	9
6	($AcrH^+ClO_4^-$)	H_2O_2	450 W high-pressure mercury lamp in a Pyrex flask (>320 nm)	20	92	-/-	-	10

Section S3 Supplementary Figures Section

1. Supplementary figures for structure and characterization.

Fig. S2. Image of the photocatalytic reactor.

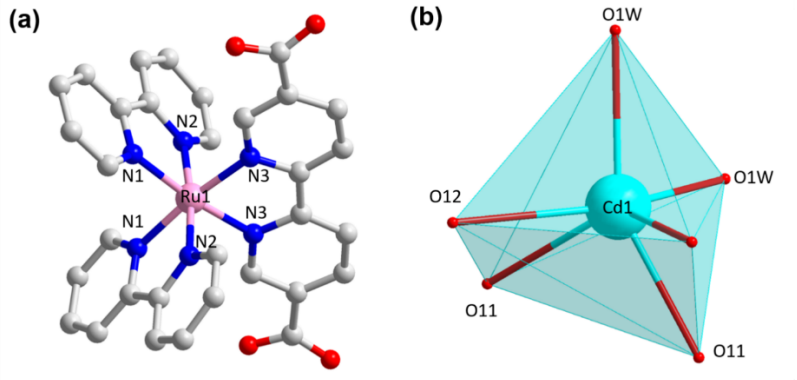

Fig. S3. The coordination modes of (a) Ru and (b) Cd.

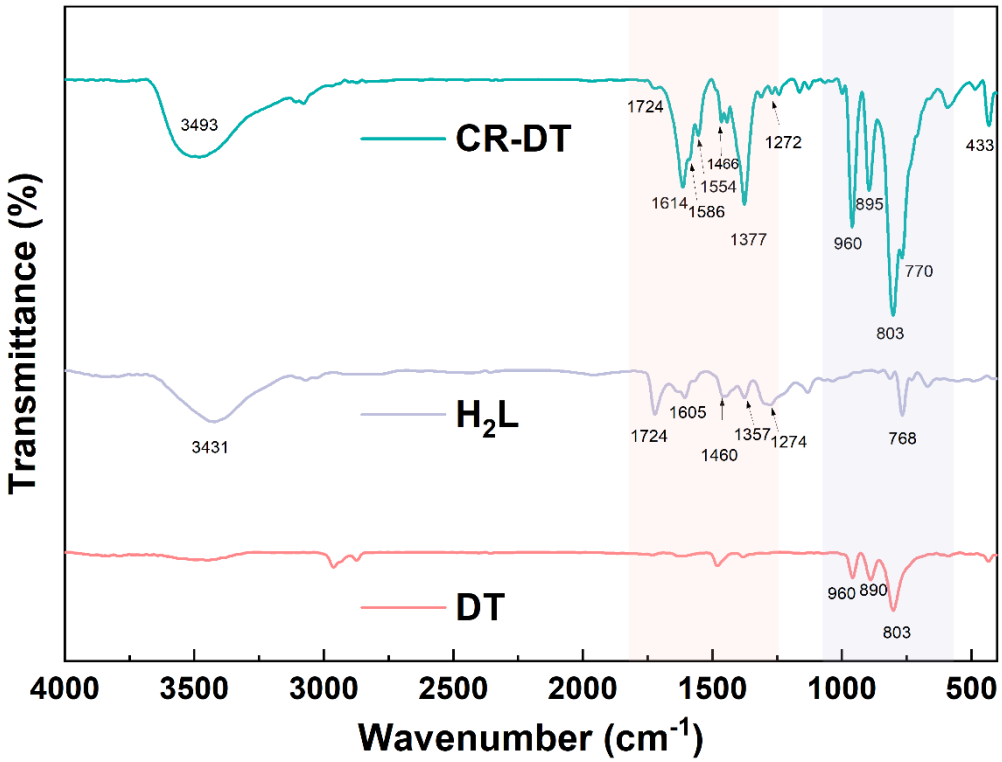

Fig. S4. The FTIR spectra of **CR-DT**, H_2L and DT.

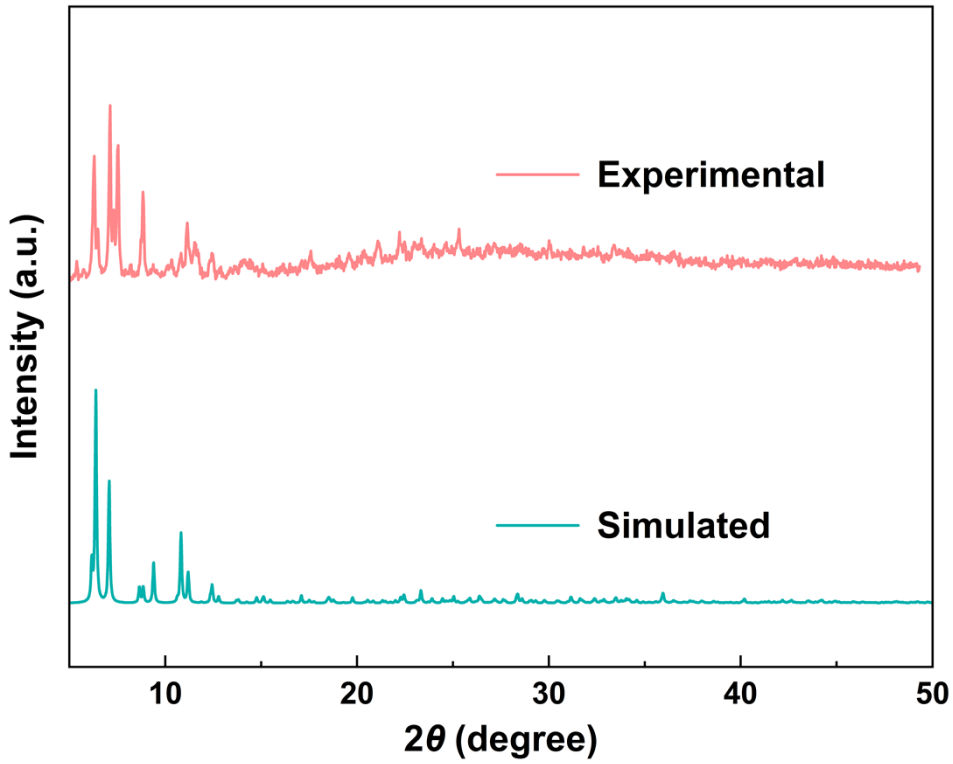

Fig. S5. The simulated and experimental PXRD patterns of **CR-DT**. The *Mercury* simulation revealed that the peak of CR-DT was very strong within the range of 5-10°. For DT, the d value is approximately around 10-11 Å. According to the Bragg equation: $n\lambda = 2d \sin\theta$, when the interplanar spacing d is very large, the corresponding diffraction angle 2θ will be very small.[11]

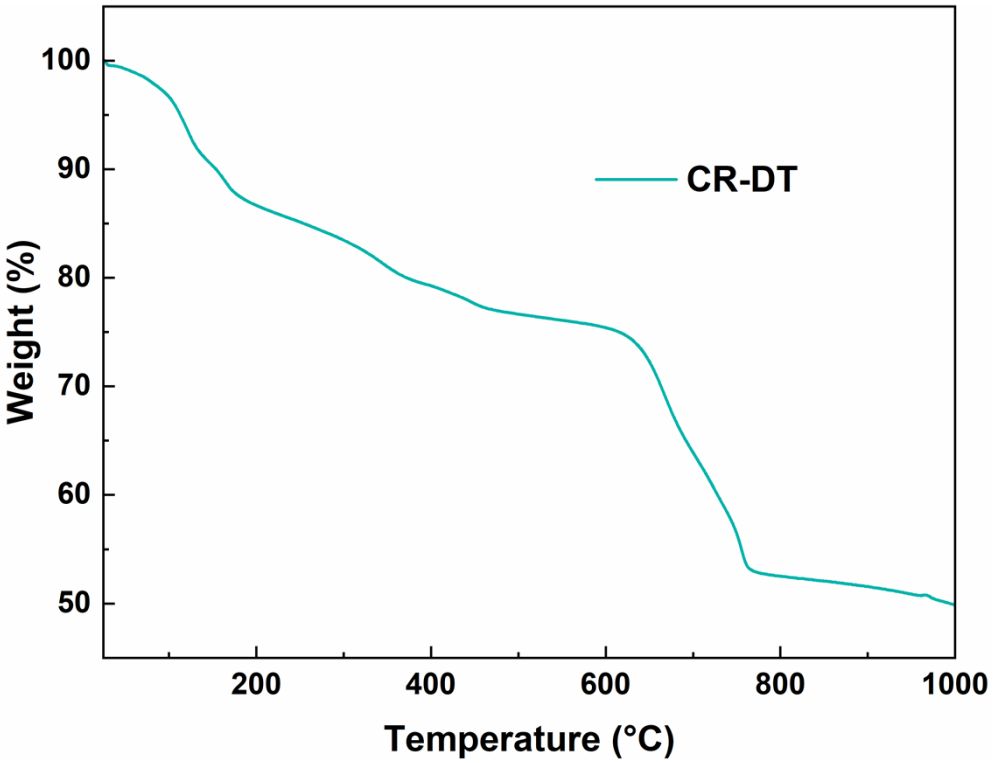

Fig. S6. The TGA curves of **CR-DT** under flowing N_2 atmosphere. It is shown that **CR-DT** has three stages of weight loss. First, the weight loss of 8.682% (calc. 8.657% with 19 H_2O) in the range of RT−140 °C.[12] The second stage is a weight loss of 15.252% at 140−540 °C, corresponding to the decomposition of organic ligands. Subsequent heating of the POMs further collapses the anion skeleton.

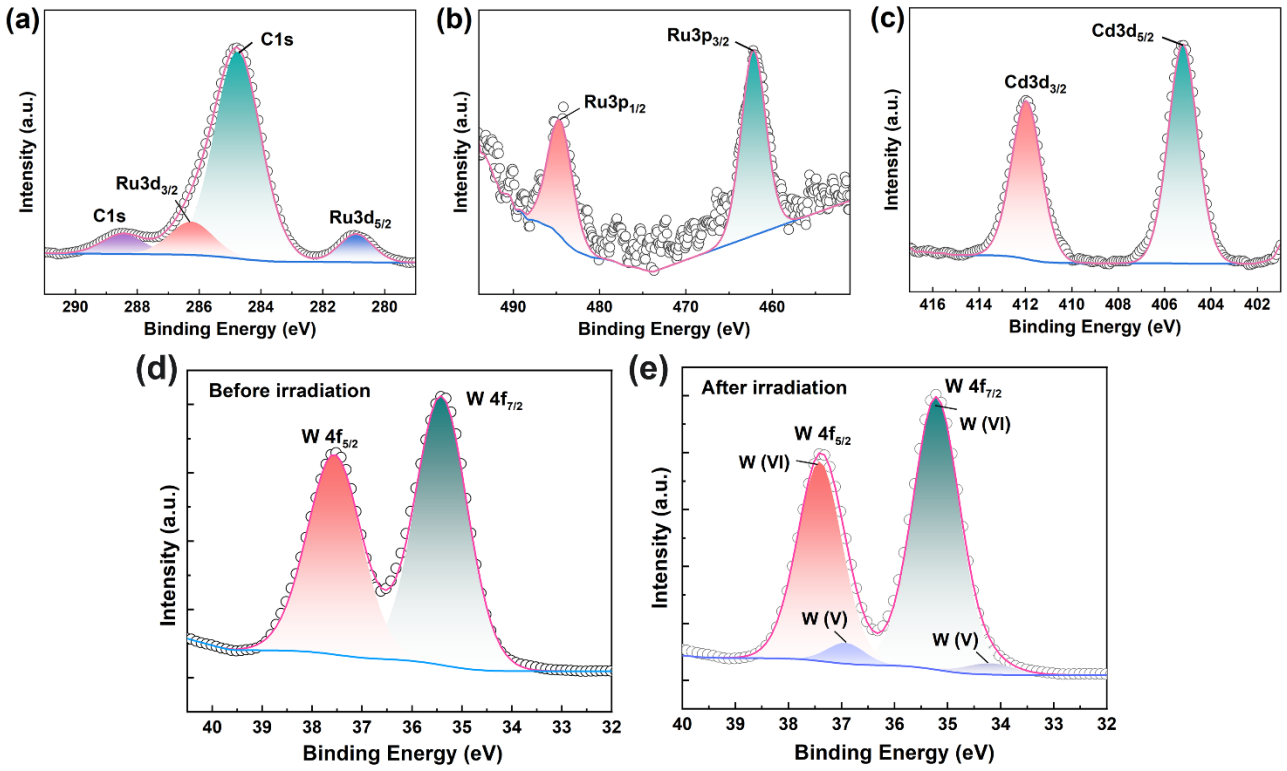

Fig. S7. XPS spectra of **(a)** C 1s& Ru 3d; **(b)** Ru 3p; **(c)** Cd 3d; and **(d)** before and **(e)** after irradiation W 4f of **CR-DT**.

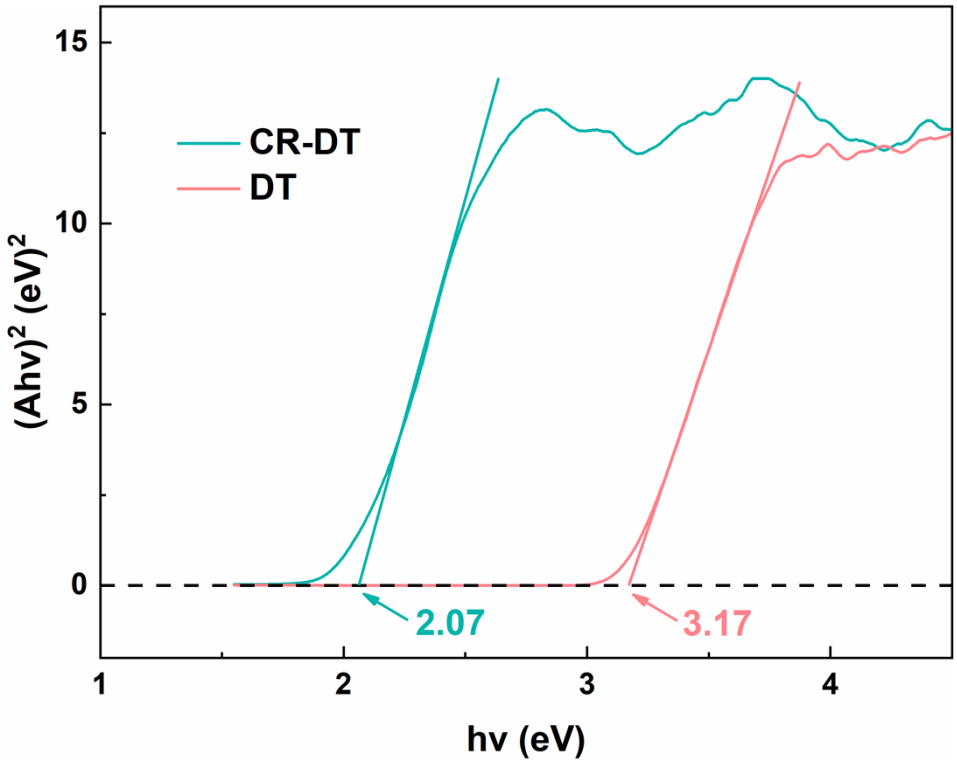

Fig. S8. The estimated energy band gaps [$(\alpha hv)^2$ vs hv] of **CR-DT**.

2. The NMR data of the lactone products listed in Table 2.[6,13,14]

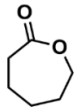

ε-caprolactone: ^{1}H NMR (500 MHz, Chloroform-*d*, ppm) δ 4.11 (dd, *J* = 6.0, 2.8 Hz, 1H), 2.55 – 2.50 (m, 1H), 1.78 – 1.72 (m, 1H), 1.69 – 1.62 (m, 2H). ^{13}C NMR (126 MHz, Chloroform-*d*) δ 176.27, 69.35, 34.59, 29.33, 28.97, 22.98.

δ-butyrolactone: ^{1}H NMR (500 MHz, Chloroform-*d*, ppm) δ 4.33 – 4.24 (m, 2H), 2.43 (t, *J* = 8.1 Hz, 2H), 2.20 (p, *J* = 7.6 Hz, 2H). ^{13}C NMR (126 MHz, Chloroform-*d*) δ 178.15, 68.75, 27.96, 22.29.

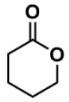

δ-valerolactone: ^{1}H NMR (500 MHz, Chloroform-*d*, ppm) δ 4.23 (t, J = 5.3 Hz, 1H), 2.44 (t, J = 6.4 Hz, 1H), 1.78 (ddt, J = 27.3, 11.8, 5.4 Hz, 2H). ^{13}C NMR (126 MHz, Chloroform-*d*) δ 171.45, 69.50, 29.88, 22.35, 19.13.

4-oxahomoadamantan-5-one: ^{1}H NMR (500 MHz, Chloroform-*d*, ppm) δ 4.42 (t, *J* = 2.4 Hz, 1H), 3.01 (s, 1H), 2.02 (d, *J* = 24.3 Hz, 2H), 1.97 – 1.84 (m, 6H), 1.80 – 1.74 (m, 2H), 1.71 – 1.65 (m, 2H), 1.20 (d, *J* = 10.6 Hz, 1H). ^{13}C NMR (126 MHz, Chloroform-d) δ 179.14, 73.34, 41.42, 35.96, 34.00, 31.15, 26.04.

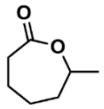

6-methyl-*ε*-caprolactone: ^{1}H NMR (500 MHz, Chloroform-*d*, ppm) δ 4.33 (p, *J* = 6.5 Hz, 1H), 2.51 (td, *J* = 13.4, 3.9 Hz, 2H), 1.85 – 1.72 (m, 3H), 1.53 – 1.39 (m, 3H), 1.21 (d, *J* = 6.5 Hz, 3H). ^{13}C NMR (126 MHz, Chloroform-d) δ 175.91, 67.75, 36.24, 35.03, 28.27, 22.93, 22.61.

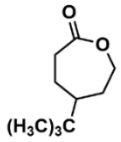

4-*tert*-butyl-*ε*-caprolactone: ^{1}H NMR (500 MHz, Chloroform-*d*, ppm) δ 4.11 – 3.98 (m, 1H), 3.95 (t, *J* = 8.1 Hz, 1H), 2.43 – 2.30 (m, 1H), 2.20 (dd, *J* = 15.9, 9.8 Hz, 1H), 1.87 – 1.71 (m, 2H), 1.36 – 1.24 (m, 2H), 0.83 (d, *J* = 2.9 Hz, 9H). ^{13}C NMR (126 MHz, Chloroform-*d*) δ 173.78, 68.84, 64.78, 44.87, 34.18, 34.04, 30.18, 27.71, 26.82, 23.97.

3. Copy of ^{1}H NMR and ^{13}C NMR spectra for the products.

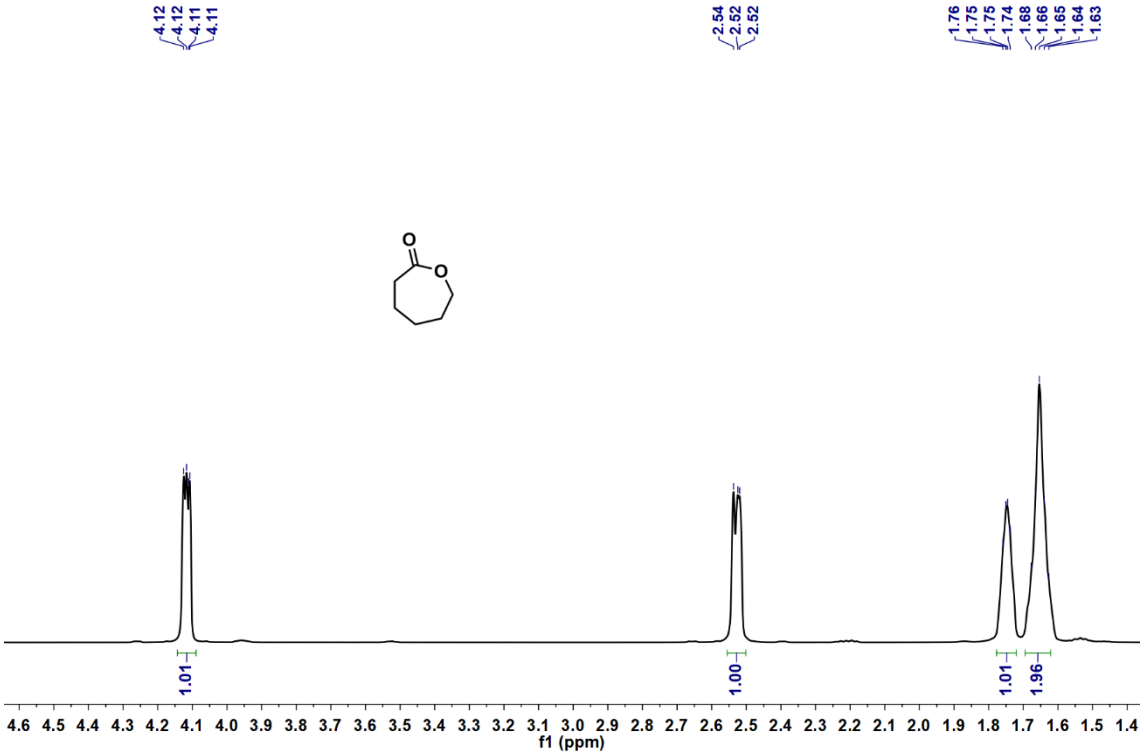

Fig. S9. ^{1}H NMR spectrum for ***ε*-caprolactone** in $CDCl_3$ (500 MHz).

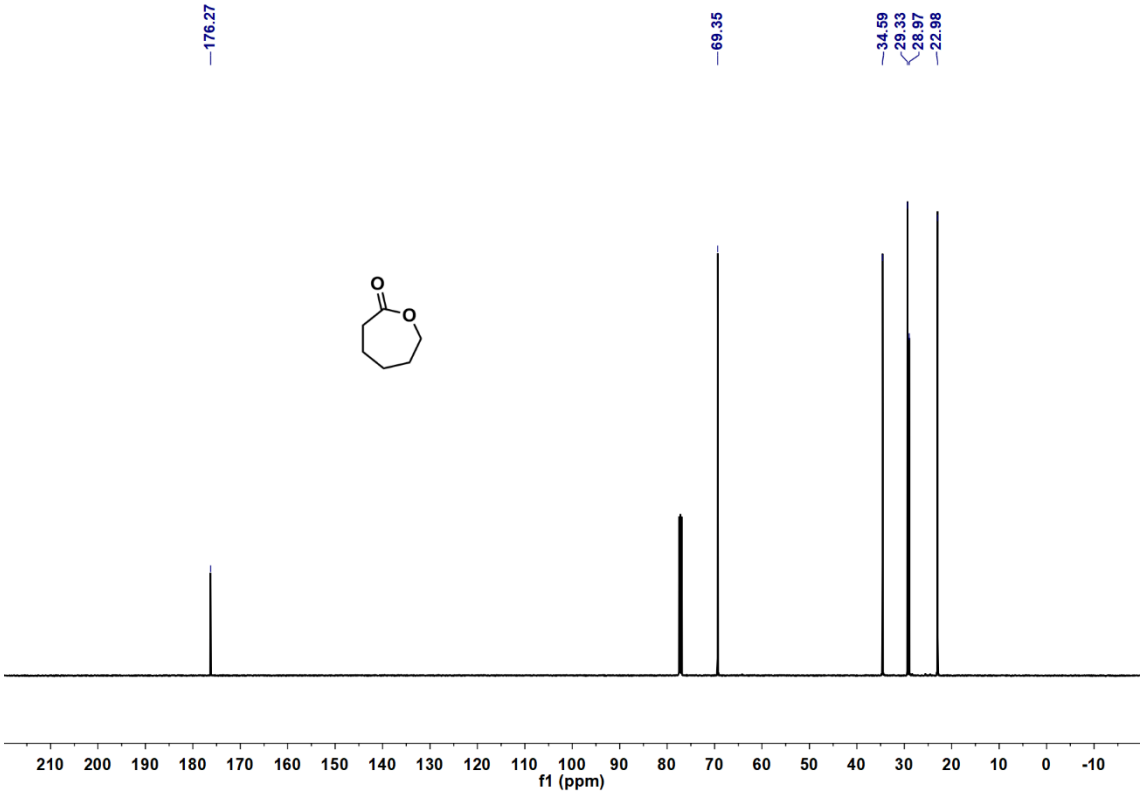

Fig. S10. ^{13}C NMR spectrum for ***ε*-caprolactone** in $CDCl_3$ (126 MHz).

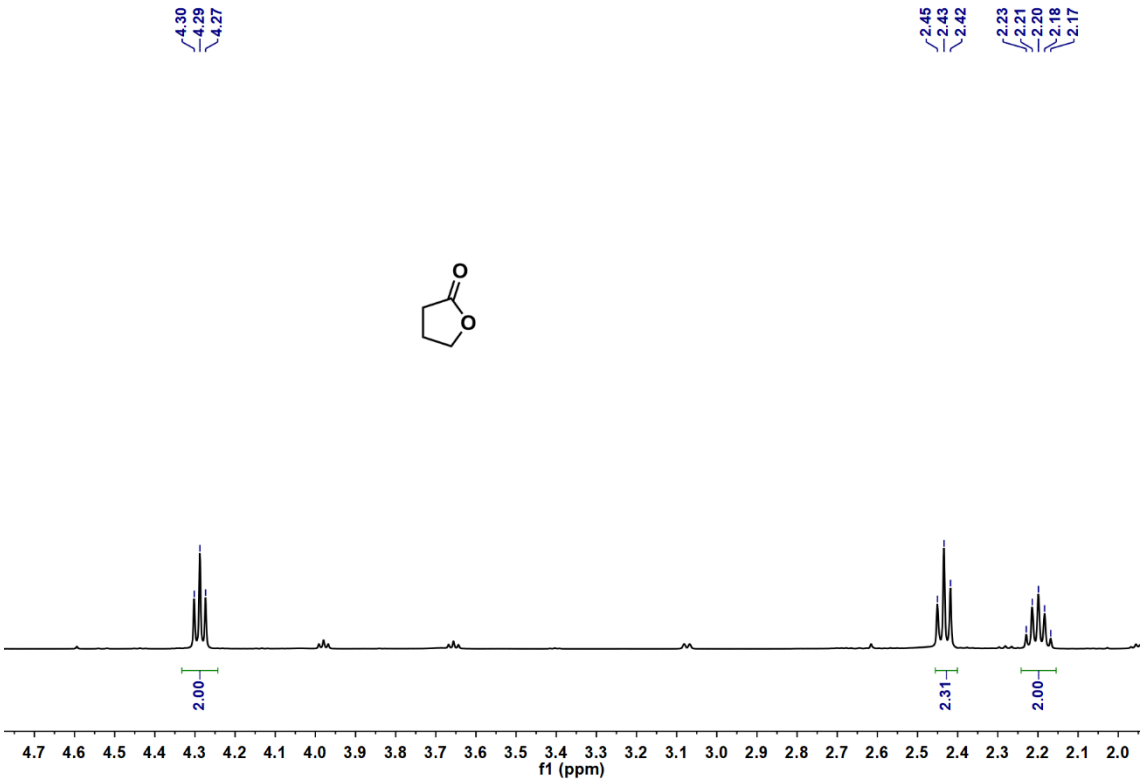

Fig. S11. ^{1}H NMR spectrum for ***δ*-butyrolactone** in $CDCl_3$ (500 MHz).

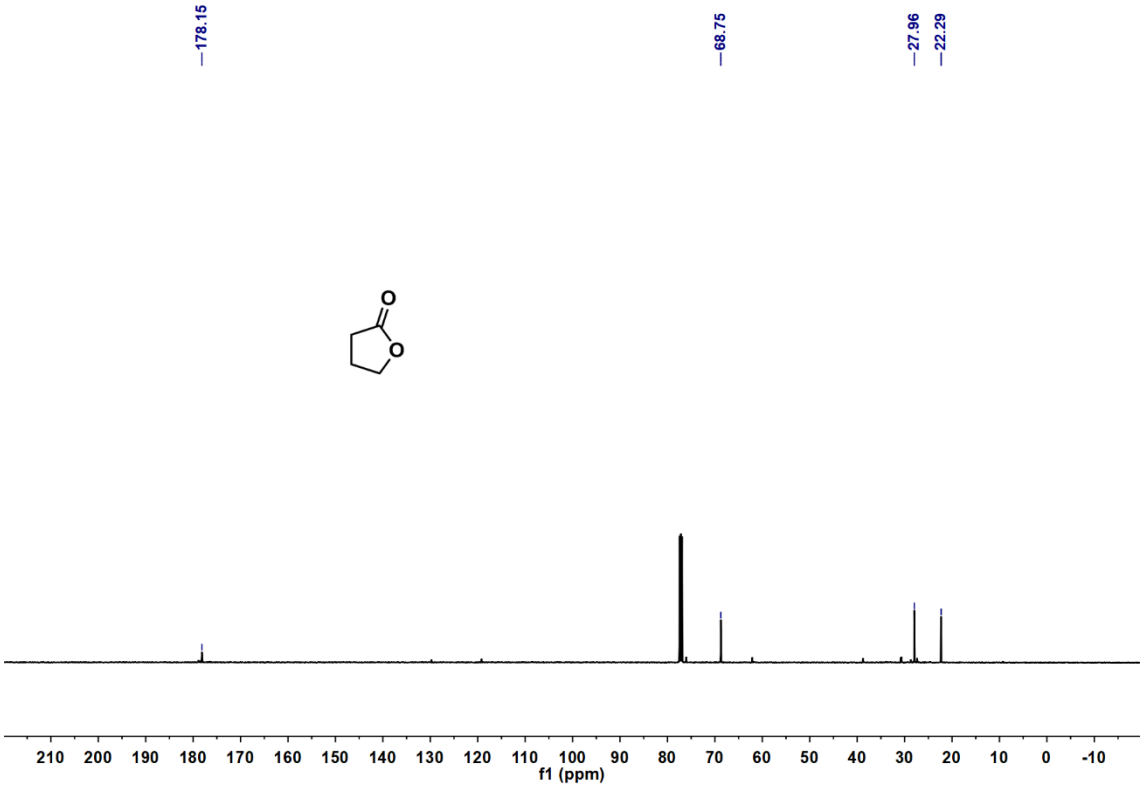

Fig. S12. ^{13}C NMR spectrum for ***δ*-butyrolactone** in $CDCl_3$ (126 MHz).

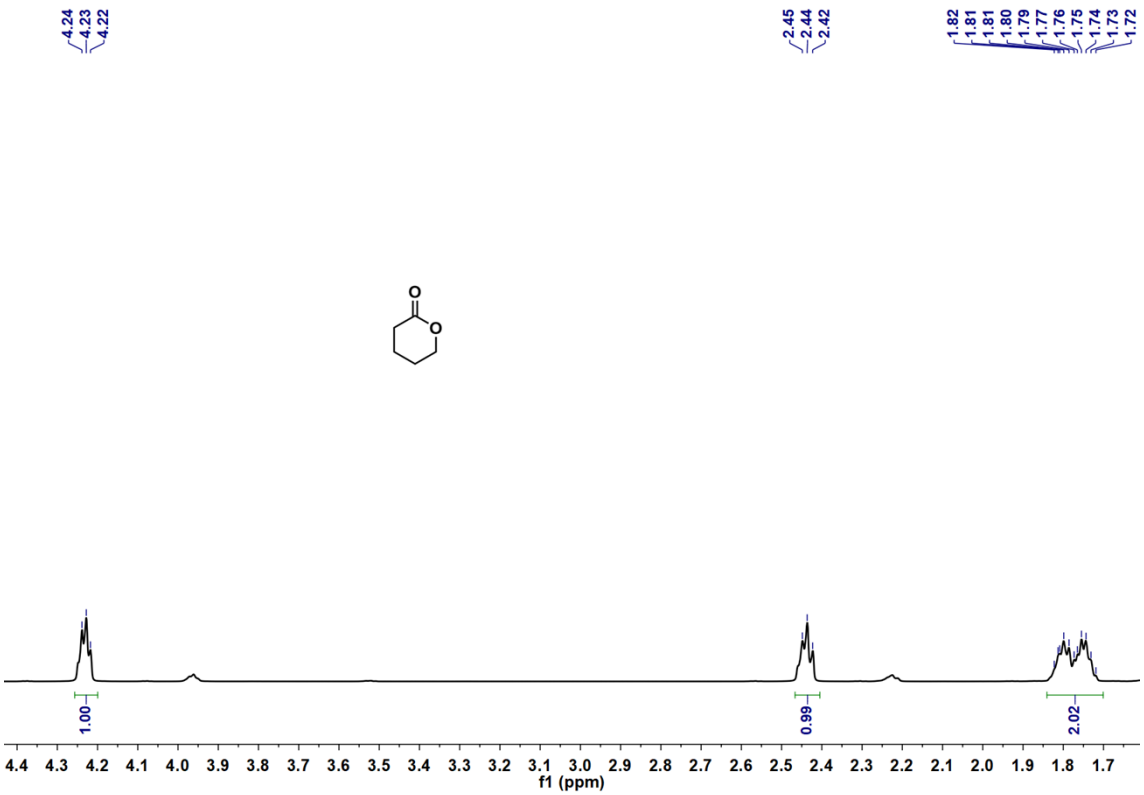

Fig. S13. ^{1}H NMR spectrum for ***δ*-valerolactone** in $CDCl_3$ (500 MHz).

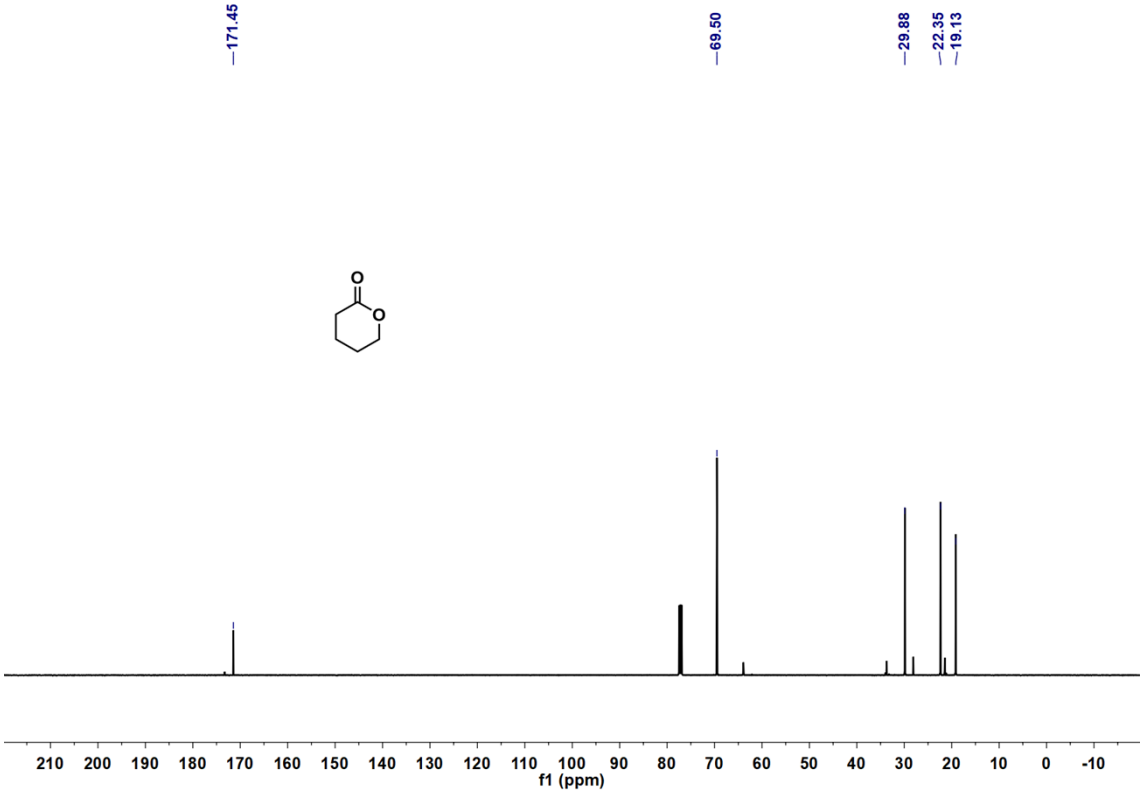

Fig. S14. ^{13}C NMR spectrum for ***δ*-valerolactone** in $CDCl_3$ (126 MHz).

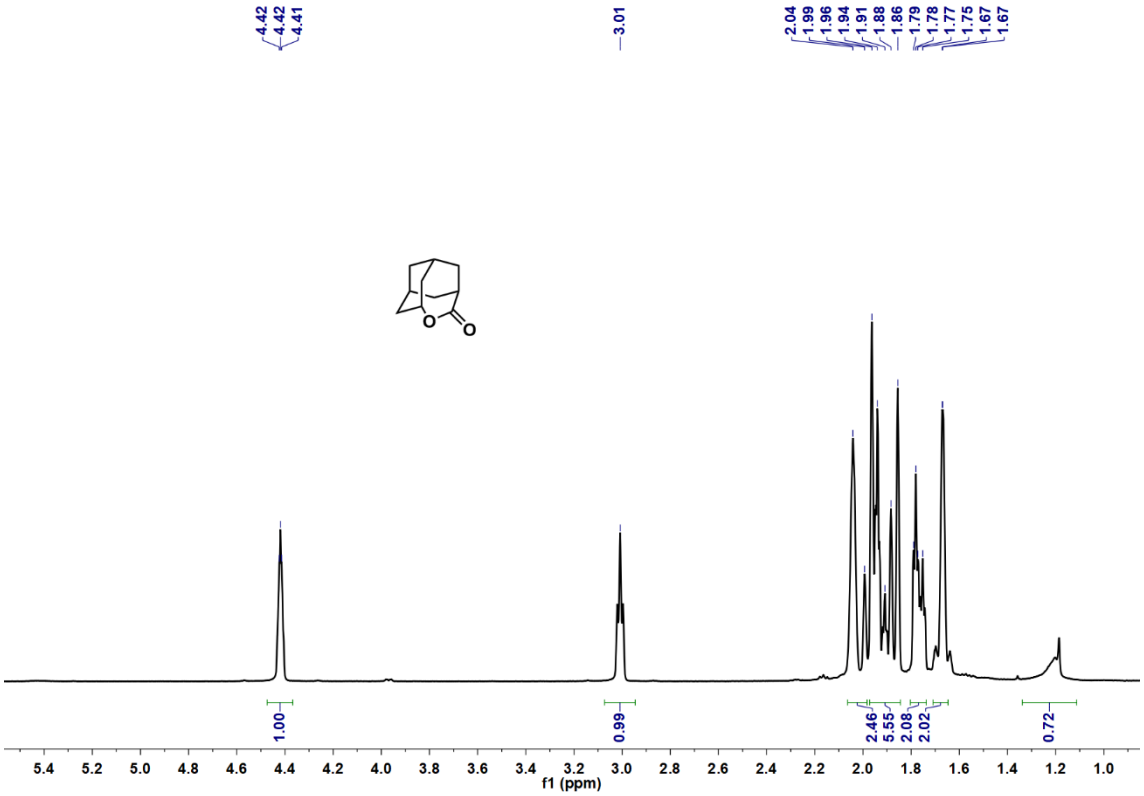

Fig. S15. ^{1}H NMR spectrum for **4-oxahomoadamantan-5-one** in $CDCl_3$ (500 MHz).

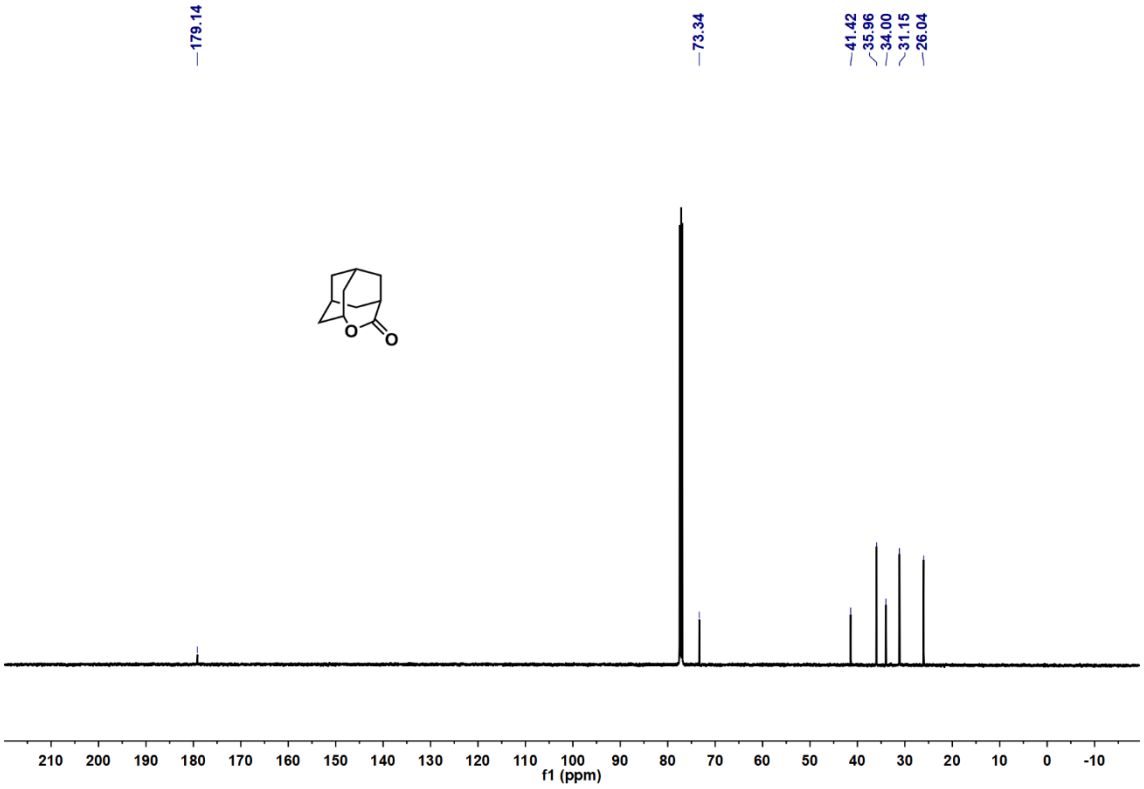

Fig. S16. ^{13}C NMR spectrum for **4-oxahomoadamantan-5-one** in $CDCl_3$ (126 MHz).

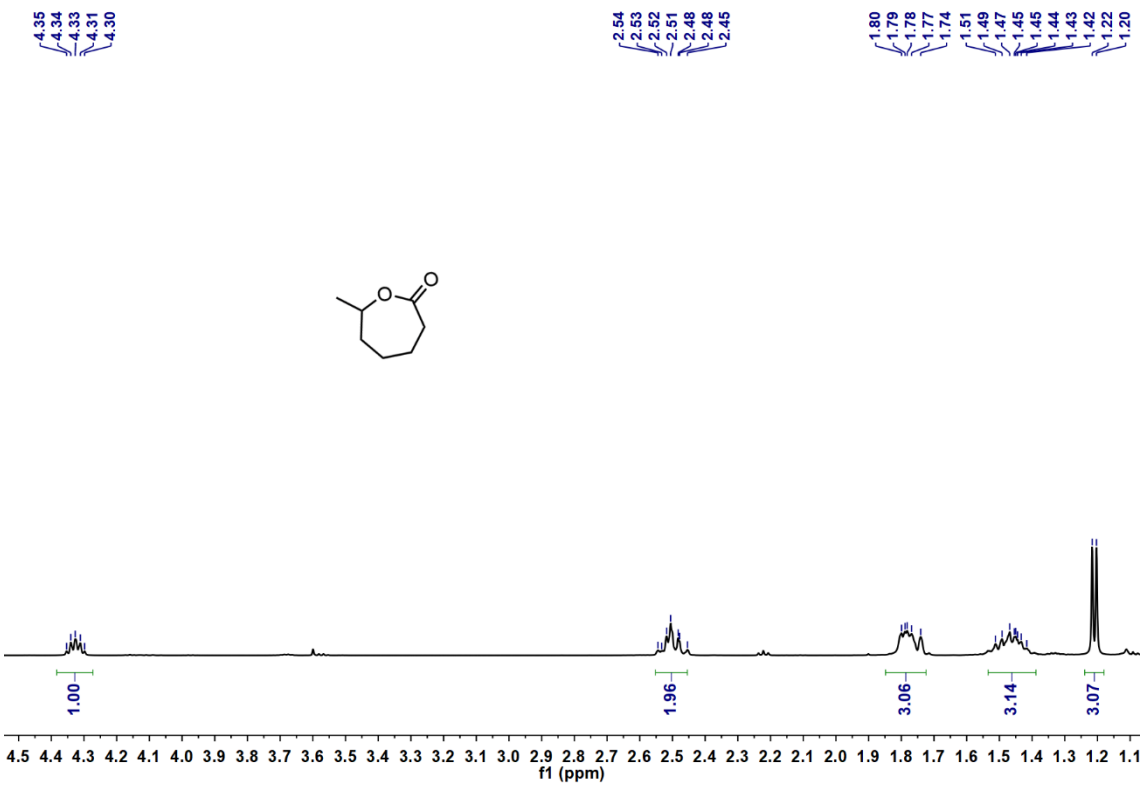

Fig. S17. ^{1}H NMR spectrum for **6-methyl-ε-caprolactone** in $CDCl_3$ (500 MHz).

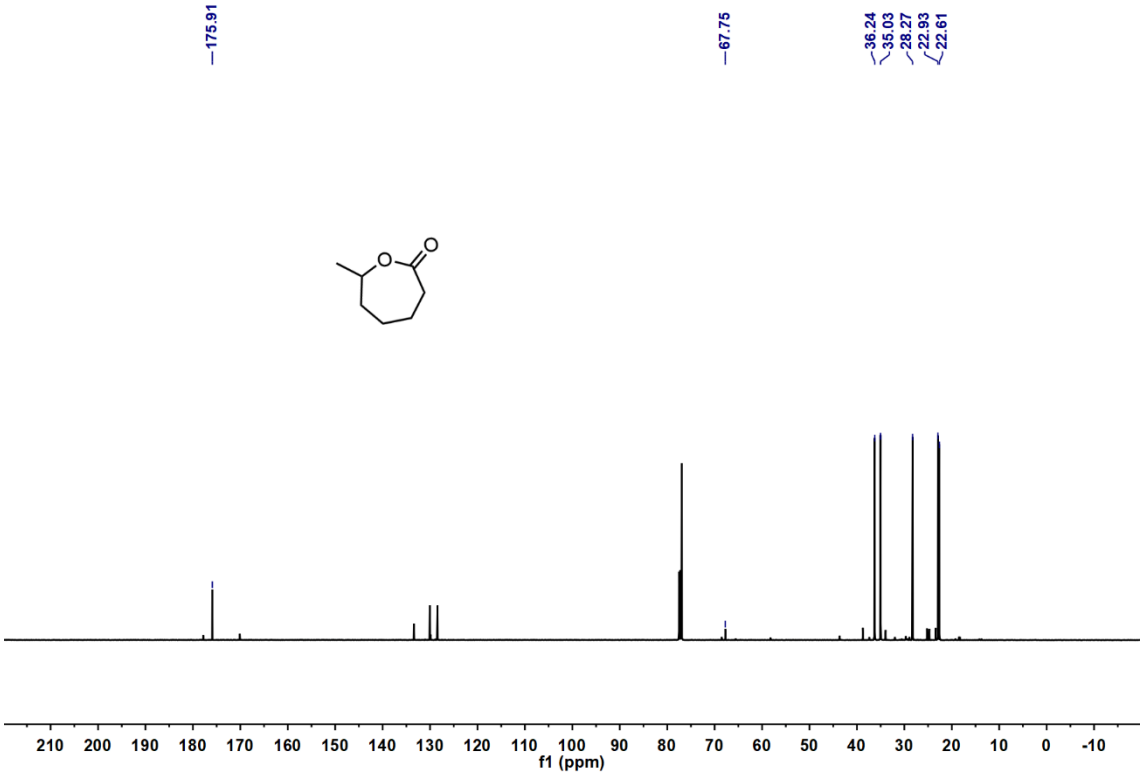

Fig. S18. ^{13}C NMR spectrum for **6-methyl-ε-caprolactone** in $CDCl_3$ (126 MHz).

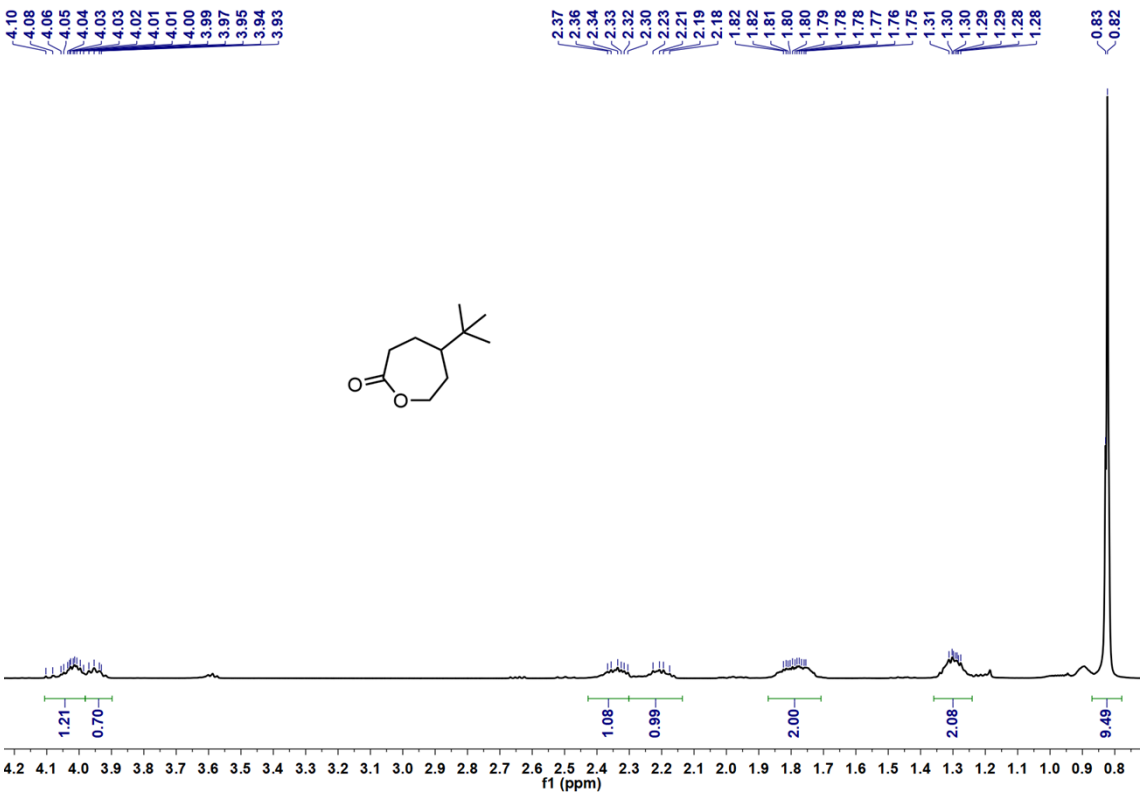

Fig. S19. ^{1}H NMR spectrum for **4-*tert*-butyl-*ε*-caprolactone** in $CDCl_3$ (500 MHz).

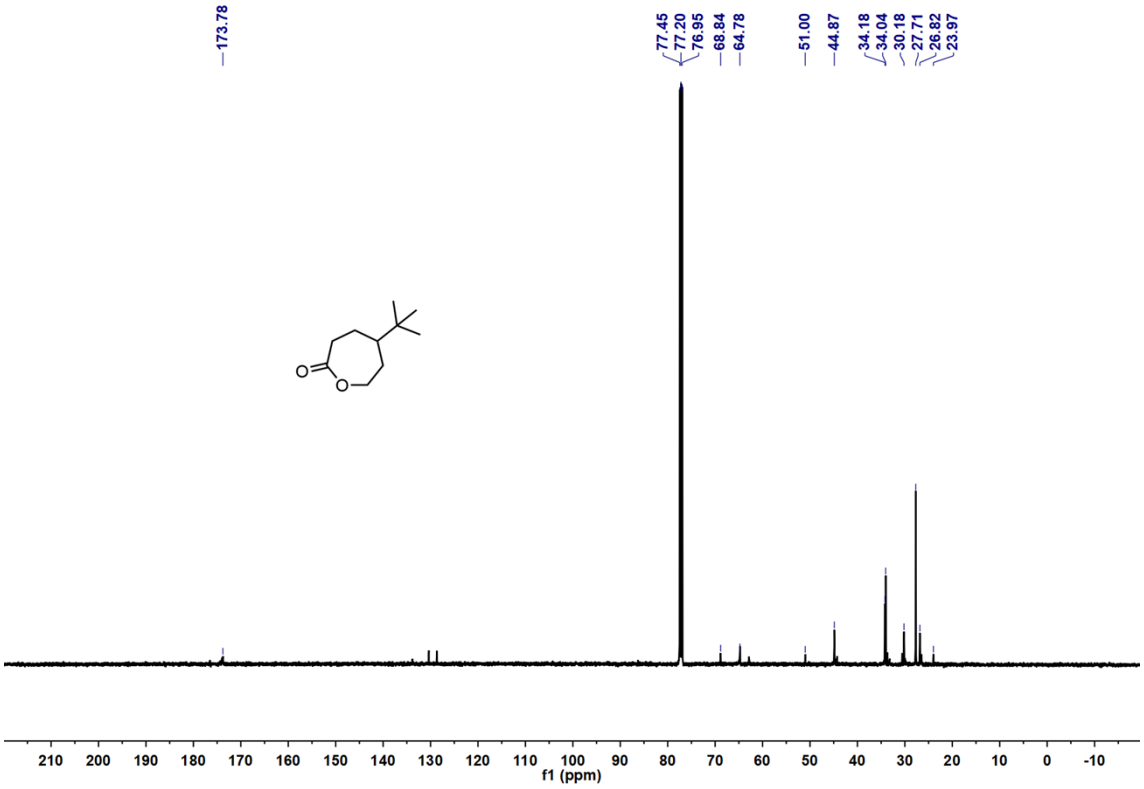

Fig. S20. ^{13}C NMR spectrum for **4-*tert*-butyl-*ε*-caprolactone** in $CDCl_3$ (126 MHz).

4. Supplementary catalytic experiments characterization diagram.

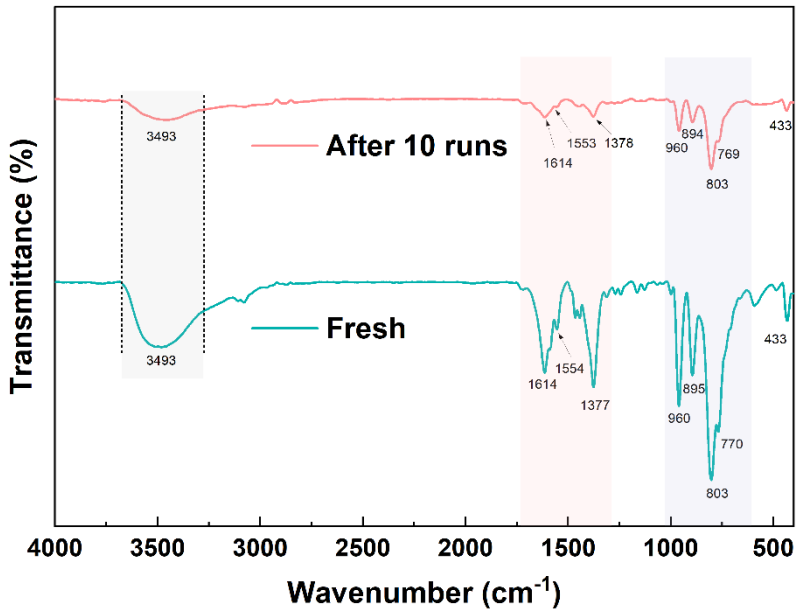

Fig. S21. The FTIR spectra of catalysts **CR-DT** before and after photocatalysis.

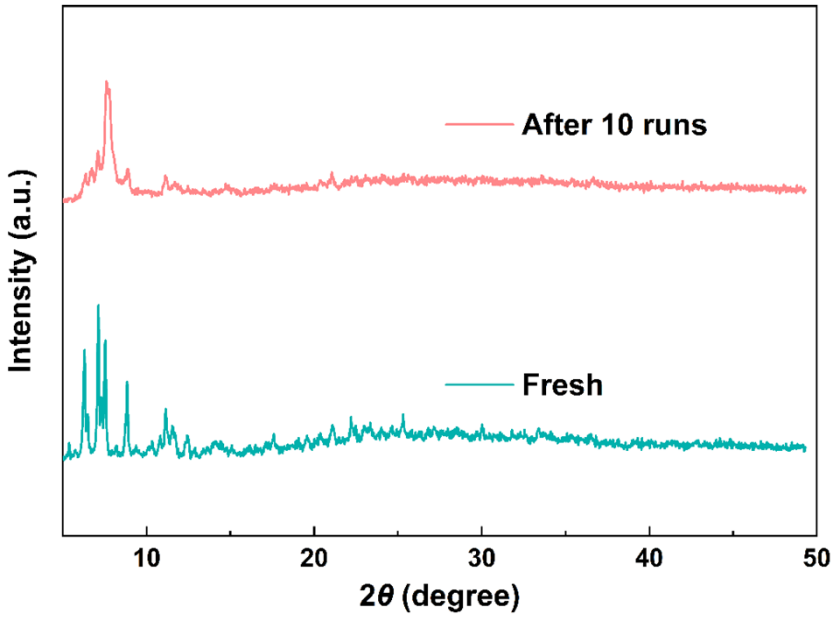

Fig. S22. The PXRD patterns of **CR-DT** in experimental and after the photocatalytic reaction.

References

(1) Shi, D.; He, C.; Sun, W.; Ming, Z.; Meng, C.; Duan, C. A Photosensitizing Decatungstate-Based MOF as Heterogeneous Photocatalyst for the Selective C–H Alkylation of Aliphatic Nitriles. *Chem. Commun.* **2016**, *52* (25), 4714–4717. https://doi.org/10.1039/C6CC00862C.

(2) Shi, D.; Zeng, L.; Ming, Z.; He, C.; Meng, C.; Duan, C. A Breathing MOF: Direct Crystallographic Observation of the Site-Selective C(Sp^3)–H Functionalization. *RSC Adv.* **2016**, *6* (57), 51936–51940. https://doi.org/10.1039/C6RA07100G.

(3) Sheldrick, G. M. Crystal Structure Refinement with *SHELXL*. *Acta Crystallogr C Struct Chem* **2015**, *71* (1), 3–8. https://doi.org/10.1107/S2053229614024218.

(4) Wang, C.; Xie, Z.; deKrafft, K. E.; Lin, W. Doping Metal–Organic Frameworks for Water Oxidation, Carbon Dioxide Reduction, and Organic Photocatalysis. *J. Am. Chem. Soc.* **2011**, *133* (34), 13445–13454. https://doi.org/10.1021/ja203564w.

(5) Hou, C.-C.; Li, T.-T.; Cao, S.; Chen, Y.; Fu, W.-F. Incorporation of a $[Ru(dcbpy)(bpy)_2]^{2+}$ Photosensitizer and a $Pt(Dcbpy)Cl_2$ Catalyst into Metal–Organic Frameworks for Photocatalytic Hydrogen Evolution from Aqueous Solution. *J. Mater. Chem. A* **2015**, *3* (19), 10386–10394. https://doi.org/10.1039/C5TA01135C.

(6) Liu, Y.; Wang, J.; Li, L.; Meng, S.; Ji, K.; Ma, P.; Wang, J.; Niu, J. Enhanced Photoinduced Baeyer–Villiger Oxidation of Ketones by Introducing Trinuclear Ruthenium Clusters into Polyoxometalate-Based Metal–Organic Frameworks. *Chem. Mater.* **2023**, *35* (10), 3941–3950. https://doi.org/10.1021/acs.chemmater.3c00120.

(7) Wang, J.; Li, L.; Liu, Y.; Yuan, Z.; Meng, S.; Ma, P.; Wang, J.; Niu, J. Intensifying Photocatalytic Baeyer–Villiger Oxidation of Ketones with the Introduction of Ru Metalloligands and Bimetallic Units in POM@MOF. *Inorg. Chem.* **2024**, *63* (16), 7325–7333. https://doi.org/10.1021/acs.inorgchem.4c00217.

(8) Li, L.; Liu, Y.; Wang, J.; Cai, M.; Liu, S.; Ma, P.; Wang, J.; Niu, J. Ru Metalloligands Participate in the Construction of POM@MOF for Enhancing the Visible Photoinduced Baeyer–Villiger Oxidation Reaction. *Inorg. Chem.* **2024**, *63* (52), 24506–24516. https://doi.org/10.1021/acs.inorgchem.4c03064.

(9) Yuan, Z.; Wang, J.; Li, H.; Li, L.; Ma, P.; Wang, J.; Niu, J. Visible-Light-Responsive Tetranuclear Ir-Based Polyoxometalates Achieve Photocatalytic Baeyer–Villiger Oxidation of Ketones. *Inorg. Chem.* **2025**, *64* (12), 5846–5855. https://doi.org/10.1021/acs.inorgchem.4c03410.

(10) Xu, H.-J.; Zhu, F.-F.; Shen, Y.-Y.; Wan, X.; Feng, Y.-S. Baeyer–Villiger Oxidation of Cyclobutanones with 10-Methylacridinium as an Efficient Organocatalyst. *Tetrahedron* **2012**, *68* (22), 4145–4151. https://doi.org/10.1016/j.tet.2012.03.108.

(11) Pope, C. G. X-Ray Diffraction and the Bragg Equation. *J. Chem. Educ.* **1997**, *74* (1), 129. https://doi.org/10.1021/ed074p129.

(12) Liu, Y.; Wang, J.; Ji, K.; Meng, S.; Luo, Y.; Li, H.; Ma, P.; Niu, J.; Wang, J. Construction of Polyoxometalate-Based Metal−organic Frameworks through Covalent Bonds for Enhanced Visible Light-Driven Coupling of Alcohols with Amines. *Journal of Catalysis* **2022**, *416*, 149–156. https://doi.org/10.1016/j.jcat.2022.10.024.

(13) Yang, Z.; Niu, L.; Ma, Z.; Ma, H.; Lei, Z. Fabrication of Highly Active Sn/W Mixed Transition-Metal Oxides as Solid Acid Catalysts. *Transition Met Chem* **2011**, *36* (3), 269–274. https://doi.org/10.1007/s11243-011-9465-3.

(14) Tang, Z.; Xiao, J.; Li, F.; Ma, Z.; Wang, L.; Niu, F.; Sun, X. Cobalt-Tetraamide-Phthalocyanine Immobilized on Fe_3O_4 /Chitosan Microspheres as an Efficient Catalyst for Baeyer–Villiger Oxidation. *ACS Omega* **2020**, *5* (18), 10451–10458. https://doi.org/10.1021/acsomega.0c00443.